Unprecedented quinoid-donor-acceptor strategy to boost carrier mobilities of semiconducting polymers for organic field-effect transistors

Journal:	*Journal of Materials Chemistry A*
Manuscript ID	TA-ART-07-2021-006383.R1
Article Type:	Paper
Date Submitted by the Author:	27-Sep-2021
Complete List of Authors:	Liu, Cheng; Guizhou University Liu, Xuncheng; Guizhou University, Zheng, Guohui; Guizhou University, Physics Gong, Xiu; Guizhou University, College of Physics Yang, Chen; Guizhou University Liu, Haizhen; South China University of Technology Zhang, Lianjie; South China University of Technology Institute of Polymer Optoelectronic Materials and Devices, Anderson, Christopher; University of California Berkeley; E O Lawrence Berkeley National Laboratory He, Bo ; E O Lawrence Berkeley National Laboratory, The Molecular Foundry Xie, Lan; Guizhou University, Department of Polymer Materials and Engineering Zheng, Rongzong; Guizhou University Liang, Huanhuan; Guizhou University Zhou, Quanfeng; Guizhou University Zhang, Zesheng; South China University of Technology Institute of Polymer Optoelectronic Materials and Devices Chen, Junwu; South China University of Technology, Institute of Polymer Optoelectronic Materials and Devices Liu, Yi; E O Lawrence Berkeley National Laboratory, The Molecular Foundry

SCHOLARONE™
Manuscripts

Unprecedented quinoid-donor-acceptor strategy to boost carrier mobilities of semiconducting polymers for organic field-effect transistors

Cheng Liu,[a] Xuncheng Liu,*[a] Guohui Zheng,[b] Xiu Gong,[b] Chen Yang,[c] Haizhen Liu,[d] Lianjie Zhang,[d] Christopher L. Anderson,[e, g] Bo He,[e, f] Lan Xie,[a] Rongzong Zheng,[a] Huanhuan Liang,[a] Quanfeng Zhou,[a] Zesheng Zhang,[d] Junwu Chen*[d] and Yi Liu*[e,f]

[a] College of Materials and Metallurgy, [b] College of Physics and [c] College of Big Data and Information Engineering, Guizhou University, Guiyang 550025, China

[d] Institute of Polymer Optoelectronic Materials and Devices, State Key Laboratory of Luminescent Materials and Devices, South China University of Technology, Guangzhou 510640, China

[e] The Molecular Foundry and [f] Materials Sciences Division, Lawrence Berkeley National Laboratory, One Cyclotron Road, Berkeley, California 94720, United States

[g] Department of Chemistry, University of California, Berkeley, Berkeley, California 94720, United States

Corresponding Authors: *xcliu3@gzu.edu.cn, *psjwchen@scut.edu.cn, *yliu@lbl.gov.

Abstract: Quinoidal-aromatic conjugated polymers hold great application potential in organic field-effect transistors (OFETs). However, the development of high mobility quinoidal-aromatic conjugated polymers still lags behind the more popular donor-acceptor (D-A) conjugated polymers, mainly owing to the lack of rational design strategy and efficient building block. Herein, a novel quinoid-donor-acceptor (Q-D-A) strategy is demonstrated to modulate the energy-level and boost the charge carrier transport mobility of conjugated polymers as

opposed to the D-A system. On the basis of this strategy, a quinoidal-aromatic conjugated polymer, namely PAQM-BT, is designed and synthesized. With the combined use of quinoid, donor and acceptor units in the backbone, the resulting Q-D-A polymer PAQM-BT displays the narrowest bandgap with the deepest-lying lowest unoccupied molecular orbital (LUMO) energy level, highest backbone coplanarity, enhanced thin-film crystallinity and smallest effective hole mass ($m_h{}^*$) in comparison with the corresponding D-A polymer PT3B1 and quinoid-donor (Q-D) polymer PAQM-3T. Benefitting from the more effective intra- and inter-chain charge transport, as corroborated by experiment and theoretical calculations, OFET devices based on PAQM-BT exhibit a highly boosted hole mobility of up to 5.10 cm^2 V^{-1} s^{-1}, which is one and four orders of magnitude higher than that of PAQM-3T and PT3B1, respectively, and is among the highest for quinoidal-aromatic conjugated polymers. The potent Q-D-A strategy not only allows energy-level to be modulated but also leads to effective charge carrier transport, opening up possibilities to the development of high mobility quinoidal-aromatic conjugated polymers based on a variety of quinoids, donors, and acceptors.

1. Introduction

Semiconducting polymers have gained great attention for their application in OFETs,[1-9] organic photovoltaics (OPVs),[10-14] and other electronic devices.[15, 16] Fine-tuning of molecular structures for the modulation of frontier orbital energy levels and the realization of high charge carrier mobilities is one of the most fundamental issues for conjugated polymers.[17-20] Many strategies have been developed to improve charge carrier mobilities via finite control of interchain hopping and intrachain transport, such as rational design of novel electroactive units, side chain engineering and optimization of active layer processing and device architecture.[21-28] Among these efforts, the D-A principle has been widely adapted for rational tuning of optoelectronic properties through the hybridization of frontier orbitals of the donor and acceptor constituents.[29-35]

In addition to D-A type polymers, conjugated polymers incorporating quinoid (Q) units are receiving increasing attention for their distinctive electronic, optical and magnetic properties imbued by the unique structural features of quinoid unit.[36-38] In quinoidal-aromatic alternating polymers, facile resonance between quinoid units and electroactive aromatics leads to effective minimization of bond length alternation (BLA), which serves as an alternative mechanism to the D-A approach to reducing the bandgap.[39] In addition, this resonance often results in high coplanarity and rigidity of the polymer backbone due to increased double bond character between its cyclic π-units.[40-44] The rigidified conformation can enhance effective π-orbital overlap, increase effective conjugation length and promote π-π interchain interactions, resulting in excellent charge carrier transporting characteristics.[45] Despite the growing interest in quinoidal polymers, the available quinoid electroactive building blocks for conjugated polymers are dwarfed by the plethora of electron donors and acceptors, with the majority being pyrollidone-fused or oxindole-capped polycyclic heteroquinoids (Figure 1a).[46-49] While the incorporation of these electron-withdrawing cyclic amide units helps stabilize the chemically reactive quinoid moiety, their electron deficiency obscures the boundary between quinoids and electron acceptors. As a result, such quinoids possess low-lying LUMO energy levels and innately narrow gaps that are responsible for the overall small gap of the quinoidal-aromatic polymers.[39, 50-53]

Recently, *para*-azaquinodimethane (*p*-AQM), emerged as the smallest stable quinoidal building block that is free of annulated aromatic units or electron-withdrawing carbonyl groups.[54-57] In addition, *p*-AQM adopts a true quinoidal structure in the ground state, which is distinct from pro-quinoidal units, *e.g.*, thieno[3,4-*b*]thiophene (T*b*T).[58] Markedly different from other ground-state quinoidal building blocks (Figure 1a),[46, 53, 59, 60] *p*-AQM is neither strongly electron-rich nor electron-deficient, acting as a unique class of electroactive building blocks aside from the traditional electron donors and acceptors for tuning frontier orbital energies of conjugated polymers.[39] Early studies of *p*-AQMs have only focused on quinoid-donor (Q-D)
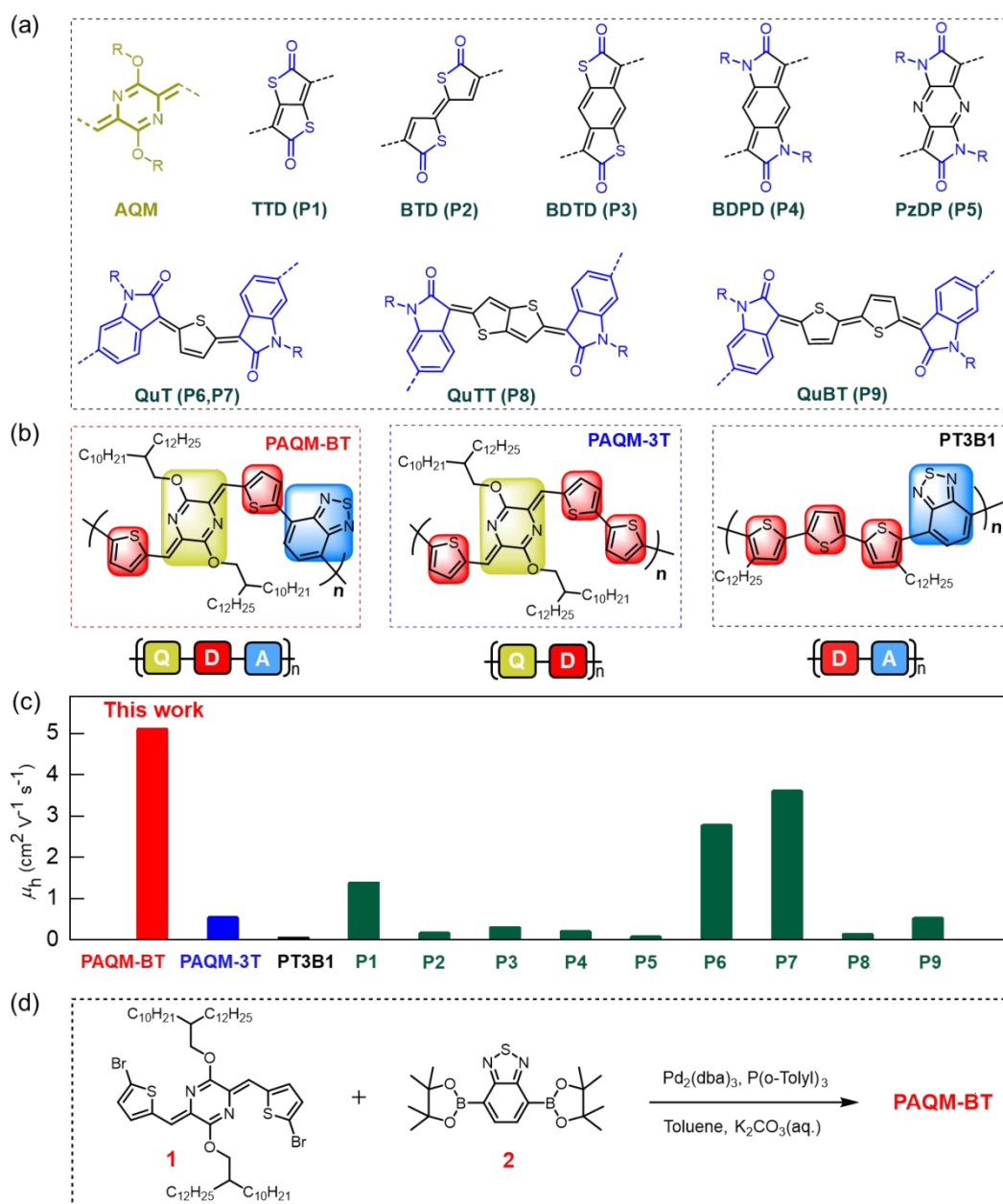
3

Figure 1. a) *p*-AQM and other typical ground-state quinoid units. Related quinoidal-aromatic polymers from the literature are listed in parentheses with structures illustrated in Figure S1. b) Molecular structures of PAQM-BT reported in this work and reference polymer PAQM-3T and PT3B1. c) A comparison of hole mobilities of PAQM-BT, PAQM-3T, PT3B1 and other quinoidal-aromatic polymers characterized by conventional spin-coating deposition methods. d) Synthetic route to PAQM-BT.

copolymers. For example, PAQM-3T, which contained *p*-AQM and terthiophene in the repeat unit and 2-decyltetradecyloxy side chains, showed an impressively low bandgap despite the

lack of obvious electron deficiency, together with a good hole mobility of 0.54 cm^2 V^{-1} s^{-1} (Figure 1b).[61] The relatively high-lying HOMO level of around −5.0 eV, however limits its potential application window. The distinct hybridization mode of the frontier orbitals in such Q-D polymers, together with the unique "charge-neutral" nature of *p*-AQM, prompted us to explore an alternative strategy for further tuning the frontier orbital energy and intrinsic carrier transport properties. Herein, we report a novel quinoid-donor-acceptor (Q-D-A) strategy by introducing an electron acceptor in the polymer repeat unit. A Q-D-A type polymer, namely, PAQM-BT, has been synthesized, which contains a *p*-AQM as the Q moiety, a weakly electron-withdrawing benzothiadiazole (BT) as the A moiety and two thiophenes as the D moiety (Figure 1b). The combined electronic effect not only results in a narrower bandgap with simultaneously lowered HOMO and LUMO energy levels, but also promotes more effective intra-chain charge transport and inter-chain charge hopping. PAQM-BT delivers an impressive hole mobility of up to 5.10 cm^2 V^{-1} s^{-1}, remarkably higher than that of the reference Q-D polymer PAQM-3T and the BT-terthiophene based D-A polymer PT3B1 (Figure 1b, c).[62]

2. Results and Discussion

2.1. Synthesis of the Polymer

The synthetic details and characterization are included in the Supplementary Information. 2-Decyltetradecyl (DT) side chain was chosen to ensure good solubility as well as to be consistent with the reference polymer PAQM-3T. Dibromo-*p*-AQM-based monomer **1** was synthesized according to the previous report in two simple steps with a good yield (Figure S2 and S3).[54] PAQM-BT was prepared by Suzuki-coupling copolymerization of monomer **1** with 4,7-bis(4,4,5,5-tetramethyl-1,3,2-dioxaborolan-2-yl)benzothiadiazole **2** at 90 °C for 3 days (Figure 1d). The purification of the polymer was conducted in air by successive Soxhlet extractions with methanol, acetone and ethyl acetate to remove impurities and finally with chloroform to afford the target product. PAQM-BT was soluble in common solvents, such as

chlorobenzene, toluene and chloroform. The molecular weight of PAQM-BT was estimated by high temperature size exclusion chromatography (SEC) at 150 °C using 1,2,4-tricholorobenzene as the eluent (Figure S4). PAQM-BT showed a number-average molecular weight (M_n) of 16.2 kDa. Thermogravimetric analysis (TGA) indicated that PAQM-BT has good thermal stability with a decomposition temperature (Td) of 367 °C at 5% weight loss (Figure S5). While PAQM-3T exhibited a phase-transition peak at 233 °C and 211 °C in the heating and cooling cycles of the differential scanning calorimetry (DSC) analysis, respectively, no obvious phase transition was observed in the temperature range of 30–300 °C for PAQM-BT (Figure S6), which implied that the backbone of PAQM-BT was more rigid than that of PAQM-3T.
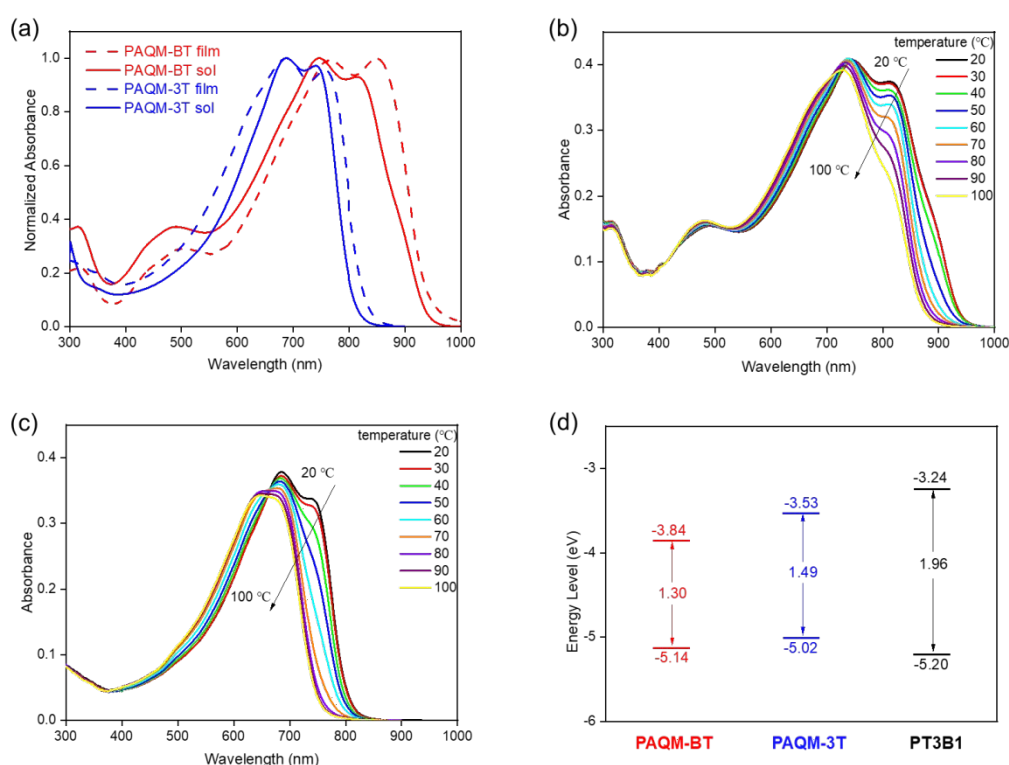

Figure 2. a) Normalized UV-vis absorption spectra of PAQM-BT and PAQM-3T in chlorobenzene and thin film at room temperature. The evolution of UV-vis absorption spectra of b) PAQM-BT and c) PAQM-3T in chlorobenzene when heated from 20 °C to 100 °C. d) Diagram of energy levels and bandgaps of PAQM-BT, PAQM-3T and PT3B1.

2.2. Optical and Optoelectronic Properties

The UV-vis absorption spectra of PAQM-BT were obtained in dilute chlorobenzene at room temperature and in thin films, as shown in Figure 2a and Table 1. Solution and thin film absorption spectra of PAQM-3T and relevant data for PT3B1 are also included for comparison. PAQM-BT exhibited significantly red-shifted absorption features in both solution and thin film compared to PAQM-3T, indicating that the insertion of the BT moiety into the backbone could enhance intramolecular charge transfer and reduce the bandgap. The solutions of both polymers displayed dual-band absorptions in the range of 600-900 nm, suggesting that there were pre-aggregated states in the solution. PAQM-BT exhibited an absorption maximum (λ_{max}) at 746 nm and a slightly lower shoulder at longer wavelength of 815 nm in solution. A redshift of ~35 nm in maximum absorption was observed from solution to film for PAQM-BT, indicating stronger intermolecular interactions in the solid state. The optical bandgap estimated from the absorption onset of the thin films of PAQM-BT was 1.30 eV, significantly smaller than the bandgap of 1.49 eV for PAQM-3T and the bandgap of 1.96 eV for PT3B1. The narrower bandgap of PAQM-BT than PAQM-3T is indicative of enhanced intra-chain and/or inter-chain interactions due to insertion of the BT moiety.[63, 64] To verify this, temperature dependent UV-vis studies of both polymers in chlorobenzene were carried out within the temperature window between 20 °C and 100 °C (Figure 2b, c). PAQM-BT displayed a gradual blue-shift of the maximum absorption peak during the heating process, which was less significant than that of PAQM-3T. Moreover, the vibronic shoulder at longer wavelength, ascribed to the interchain aggregation, was still retained at 100 °C for PAQM-BT but disappeared for PAQM-3T at only 50 °C. It is apparent that the insertion of BT moiety into the backbone leads to stronger interchain interactions, which are conducive for intermolecular charge hopping.

The frontier orbital energy levels of PAQM-BT were probed using cyclic voltammetry (CV) (Figure S7). The HOMO and LUMO energy levels for PAQM-BT were estimated to be

−5.14 eV and −3.84 eV, respectively (Figure 2d). Compared to PAQM-3T, the HOMO and

LUMO levels were lowered by 0.12 eV and 0.31 eV, respectively, while the trends were in

close agreement with the theoretical results (see Theoretical Calculations section). However,

compared to PT3B1, PAQM-BT showed a comparable HOMO energy but a significantly

lowered LUMO energy level by 0.60 eV, indicating a dramatic effect in decreasing the

energetics of LUMO by the quinoid *p*-AQM unit.

Table 1. Summary of optical and electrochemical properties of three polymers.

	Solution			Film			HOMO[b] [eV]	LUMO [eV]
	λ_{max1} [nm]	λ_{max2} [nm]	E_g[a] [eV]	λ_{max1} [nm]	λ_{max2} [nm]	E_g [eV]		
PAQM-BT	746	815	1.31	766	850	1.30[a]	−5.14	−3.84[c]
PAQM-3T[d]	687	742	1.53	688	758	1.49	−5.02	−3.53
PT3B1[e]	384	500	2.07	395	539	1.96	−5.20	−3.24

[a]Optical bandgap estimated on the basis of the absorption onset. [b]Measured by cyclic

voltammetry. [c]Calculated by subtraction of film optical bandgap from HOMO level. [d]Data

from ref 54. [e]Data from ref 62.

2.3. OFET Fabrication and Performance

To investigate the charge carrier transport properties of PAQM-BT, OFET devices with

bottom-gate top-contact (BGTC) architecture were fabricated in glove box and measured in air.

Gold (Au) was utilized as the source and drain electrodes, heavily n-doped Si was used as the

gate electrode and *n*-octadecyltrichlorosilane (OTS)-modified SiO_2 was chosen as the dielectric

layer. The semiconducting layers were all deposited by conventional spin-coating and then

annealed at 150 °C or 250 °C as noted. The fabrication details are provided in the

Supplementary Information. OFET characteristics were carried out using PDA FS-Pro

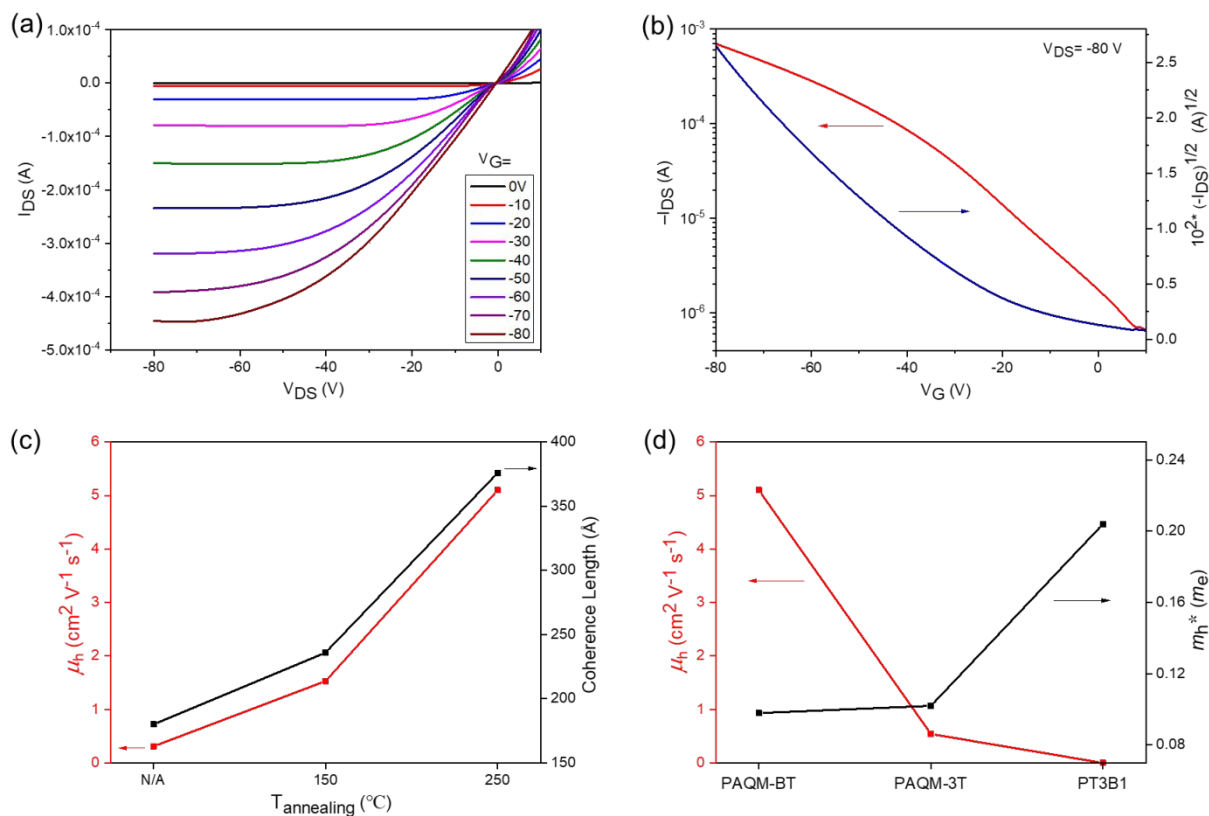semiconductor characterization system. Representative output and transfer curves and device

Figure 3. Typical a) output and b) transfer characteristics of OFETs based on PAQM-BT annealed at 250 °C. c) Hole mobilities and coherence length of PAQM-BT at different annealing temperature. d) Hole mobilities and effective hole masses of PAQM-BT, PAQM-3T and PT3B1.

performances are shown and summarized in Figure 3, Figure S8 and Table 2. For comparison, the relevant parameters of PAQM-3T and PT3B1 were also included. PAQM-BT OFET devices exhibited distinct *p*-type transporting behavior with a maximum hole mobility of 0.31 cm^2 V^{-1} s^{-1}. After thermal annealing treatment at 150 °C, PAQM-BT displayed an increased hole mobility of 1.53 cm^2 V^{-1} s^{-1}. At the thermal annealing temperature of 250 °C, the hole mobility could be further boosted to 5.10 cm^2 V^{-1} s^{-1}, which was one order of magnitude higher than that of PAQM-3T and four orders of magnitude higher than that of D-A polymer PT3B1.[54, 62] To the best of our knowledge, this hole mobility is the highest for quinoidal-aromatic conjugated polymers (Figure 1c, Table S1) except one example which shows a higher hole

mobility up to 8.09 cm^2 V^{-1} s^{-1} using an optimized and non-conventional off-center spin-coating deposition method.[45] It is clear that insertion of the BT moiety into the backbone can greatly enhance the carrier transport in the Q-D-A type polymer.

Table 2. OFET performances, coherence length and effective masses of three polymers.

Polymer	$T_{annealing}$	μ_h[a)]	V_{th}	$I_{on/off}$	Coherence Length	$m_h^*(m_e)$[c)]
	[°C]	[cm^{2}V^{-1}s^{-1}]	[V]		[Å]	
	N/A[b)]	0.31 (0.25)	−4	10^4-10^5	180	
PAQM-BT	150	1.53 (1.14)	−6	10^4-10^5	236	0.098
	250	5.10 (4.35)	−13	10^3-10^4	376	
PAQM-3T[d)]	200	0.54 (0.47)	−14	10^4-10^5	288	0.102
PT3B1[e)]	—[f)]	6.10×10^{-4}	−16	10^3-10^4	—[f)]	0.204

[a)]Maximum mobility. Average value was based on 10 independent devices and listed in parentheses. [b)]Thermal annealing was not applied. [c)]Effective hole mass (m_h^*) extracted from the theoretical calculations. m$_e$ represents the mass of an electron. [d)]Data from ref 54. [e)]Data from ref 62. [f)]Not available.

2.4. Thin-Film Morphology

The unusually high hole mobility of PAQM-BT prompted us to probe the correlation between film morphologies and charge transport. To investigate the crystallinity and molecular packing of PAQM-BT thin films, grazing-incidence wide-angle X-ray scattering (GIWAXS) measurement and atomic force microscopy (AFM) studies were conducted. GIWAXS patterns are shown in Figure 4 and the corresponding crystallographic parameters are summarized in Table 2. The as-cast film of PAQM-BT displayed a bimodal texture with both face-on and edge-on orientation as judged by the presence of (h00) and (010) diffraction peaks in the out-of-plane (OOP) direction, which was similar to the as-cast film of PAQM-3T. The crystalline coherence length (CCL) of the (100) diffraction peak was 180 Å, which represents the crystalline domain size, was calculated using the full width at half maximum (FWHM) of this (100) peak.[65] Upon

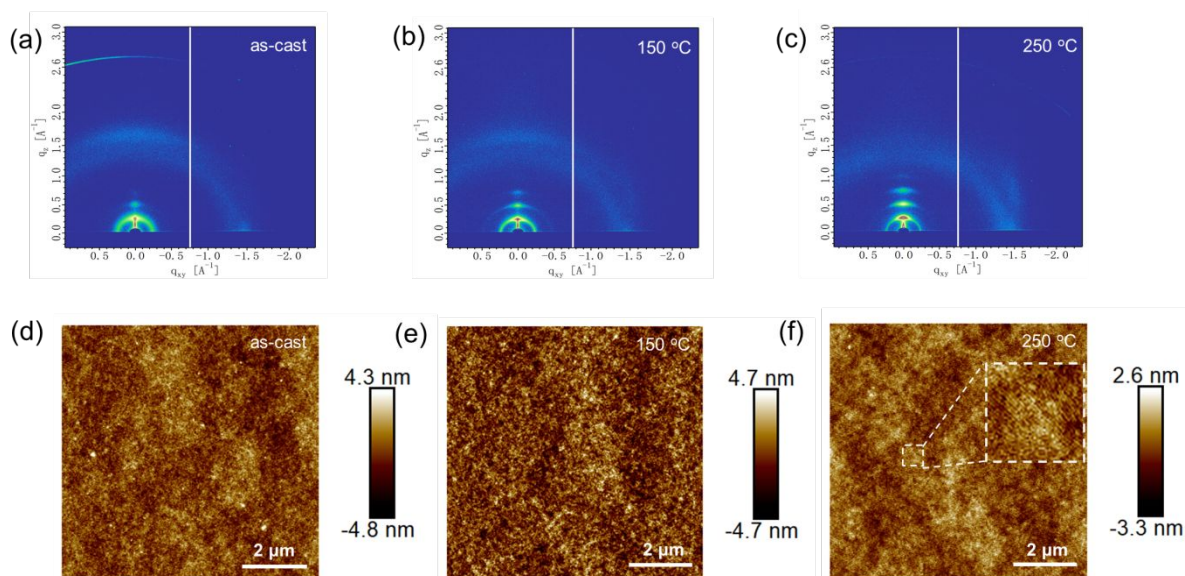thermal annealing at 150 °C, the bimodal texture was maintained with the (h00) diffraction

Figure 4. GIWAXS patterns of PAQM-BT of a) as-cast film, b) 150 °C annealed film and c) 250 °C annealed film. AFM images of PAQM-BT of d) as-cast film, e) 150 °C annealed film and f) 250 °C annealed film.

peaks becoming sharper and stronger in the OOP direction, leading to a slight increase of the (100) CCL to 236 Å, which was consistent with the improved hole mobility. Annealing at 250 °C led to further changes in the orientation and CCL of the crystallites. Higher order and strong (h00) diffraction peaks (n up to 4) together with the disappearance of (010) diffraction peak in the OOP direction clearly indicated a pure edge-on orientation in the 250 °C annealed film. The (100) CCL was further increased to 376 Å, consistent with enhanced crystallinity and highly ordered lamellar packing. The large CCL and pure edge-on orientation account for the dramatically improved hole mobility of PAQM-BT, as in-plane π-π stacking is favorable for lateral charge transport in OFETs, while the large CCL is beneficial for lowering the density of grain boundaries and facilitating charge hopping across grain boundaries.[66] Thermal annealing from low to high temperature continuously increases (100) CCL and enhances the crystallinity of PAQM-BT, which corroborates well with the successively improved hole mobilities (Figure 3c). In comparison, the annealed film of PAQM-3T showed a bimodal texture with a smaller

(100) CCL of 288 Å, and correspondingly an inferior hole mobility than that of PAQM-BT. AFM images of as-cast and annealed film of PAQM-BT are shown in Figure 4d-f. The as-cast film showed a smooth morphology and crystalline features with a root mean square (RMS) roughness of 0.82 nm. After annealing at 150 °C, PAQM-BT displayed larger crystalline grains with RMS roughness of 1.07 nm. Thermal annealing at 250 °C generated observable fiber-like networks with decreased RMS roughness of 0.56 nm, which was beneficial for the establishment of efficient charge hopping channels and improved charge hopping, in agreement with its high observed charge mobility. Moreover, side chains of conjugated polymers can largely affect interchain packing, film crystallinity, and thus charge mobility.[27] Modification of side chains on the *p*-AQM moiety to improve film crystallinity and charge mobilities for *p*-AQM-based conjugated polymers is currently under evaluation and will be reported in due course. Overall, the insertion of BT moiety into the backbone afforded larger crystalline coherence length, increased crystallinity and pure edge-on orientation, leading to more effective intermolecular hole hopping.

2.5. Theoretical Calculations

To get more in-depth understanding of the origin of the greatly improved hole mobility for PAQM-BT, theoretical calculations were performed to evaluate the chain conformation, frontier molecular orbital distributions and band structures. Relevant calculations of Q-D polymer PAQM-3T and D-A polymer PT3B1 were also carried out for comparison (Figure 5). Density functional theory (DFT) calculations of a dimer segment of each of the three polymers were performed using Gaussian 09 at the B3LYP/6-311G (d, p) level for understanding the backbone conformation and frontier molecular orbital distributions (Supplementary Information). The dimer of the *p*-AQM-BT repeat unit adopted a highly planar geometry with very small dihedral angles of ~0° between the neighboring moieties in the backbone and was significantly more planar than the dimers of both *p*-AQM-3T and BT-3T, suggesting that Q-D-

A design strategy could result in enhanced coplanarity of the backbone structure that is conducive to efficient
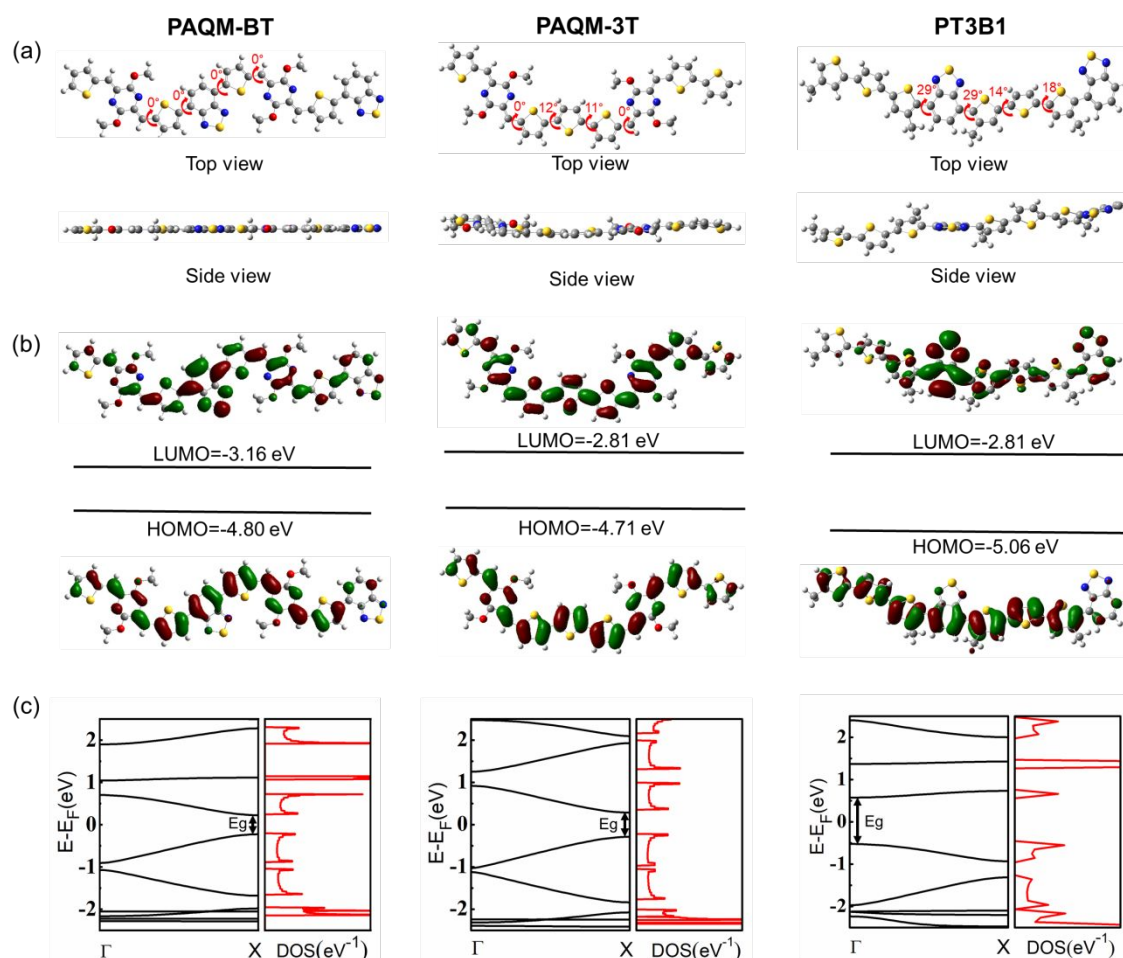

Figure 5. a) Optimized geometries of the dimeric segments of the three polymers, in which alkyl chains are substituted with methyl groups to simplify the calculation. b) Calculated molecular orbital distribution and energy levels of the dimeric segments of three polymers. c) Band structures and partial densities of states (DOS) of three polymers.

intramolecular charge transport and intermolecular charge hopping. The calculated HOMO and LUMO levels of the *p*-AQM-BT dimers were 0.09eV and 0.35eV lower than those of *p*-AQM-3T dimers, respectively. This computationally predicted trend is in good agreement with the experimental results described above. Furthermore, the HOMO and LUMO orbitals were well delocalized over the whole backbone of the *p*-AQM-BT dimer, which was also favorable for

intramolecular charge transport along the backbone. To evaluate the intramolecular charge transport along the backbone of the three polymers, we carried out theoretical calculations of their effective hole masses (m_h^*). Smaller m_h^* implies more efficient intramolecular charge transport along the backbone.[67, 68] The calculation of band structures and density of states of the polymers were performed using Vienna *ab initio* simulation package (VASP) with the Perdew-Burke-Ernzerhof (PBE) functional (Supplementary Information). Band structures, partial densities of states (DOS) and calculated m_h^* are shown and summarized in Figure 5, Figure S9 and Table 2. The calculations revealed that the bandgaps of the three polymers followed the order PAQM-BT< PAQM-3T< PT3B1, in full consistency with the experimental results. Furthermore, m_h^* was calculated to be only 0.098 m_e for PAQM-BT, being relatively small and comparable to those of polymers with efficient charge transport.[64, 68] However, PAQM-3T and PT3B1 showed larger m_h^* values of 0.102 m_e and 0.204 m_e, respectively (Figure 3d). The smallest m_h^* indicate that intramolecular hole transport in PAQM-BT was the most efficient, which contributed to the improved hole mobility in comparison to PAQM-3T and PT3B1.

3. Conclusion

In summary, we presented an unprecedented Q-D-A design strategy that is implemented in the design and synthesis of a quinoidal-aromatic polymer PAQM-BT. Compared to the previously reported Q-D polymer PAQM-3T and the D-A polymer P3TB1, the Q-D-A polymer PAQM-BT has the smallest bandgap, confirming that expanding the D-A system with additional quinoid units can bring about predictable and favorable frontier energy modulations. In addition, PAQM-BT exhibits enhanced backbone rigidity, stronger intermolecular interactions and higher crystallinity, all contributing to more effective intrachain and interchain charge transport. Theoretical calculations reveal that PAQM-BT displays a higher coplanarity and smaller m_h^* compared to PAQM-3T or P3TB1, supporting more efficient intramolecular hole transport along the polymer backbone. PAQM-BT displays an excellent hole mobility of

up to 5.10 cm^2 V^{-1} s^{-1}, which is among the highest for quinoidal-aromatic conjugated polymers. The Q-D-A strategy is expected to be applicable more generally in producing low bandgap polymers with high mobilities, well beyond the example demonstrated in this study. Considering the vastly available electron donors and acceptors, the combination of the trio (quinoids, donors, and acceptors) will may provide unlimited access to quinoidal-aromatic polymers with exceptional optoelectronic properties.

Author contributions

Cheng Liu: investigation, methodology, data curation, formal analysis, writing-review & editing. Xuncheng Liu: conceptualization, investigation, resources, funding acquisition, supervision, writing–original draft. Guohui Zheng: data curation, software, methodology. Xiu Gong: data curation, methodology, resources. Chen Yang: data curation, software. Haizhen Liu: software, methodology. Lianjie Zhang: methodology, resources. Christopher L. Anderson: writing–review & editing. Bo He: resources. Lan Xie: resources. Rongzong Zheng: resources. Huanhuan Liang: resources. Quanfeng Zhou: resources. Zesheng Zhang: formal analysis. Junwu Chen: formal analysis, investigation, resources, funding acquisition. Yi Liu: conceptualization, methodology, funding acquisition, writing–review & editing.

Conflicts of interest

The authors declare that they have no known competing financial interests or personal relationships that could have appeared to influence the work reported in this paper.

Acknowledgements

Electronic supplementary information (ESI)

Supplementary data to this article can be found online.

References

1.   T. L. D. Tam, M. Lin, A. D. Handoko, T. T. Lin and J. Xu, *J. Mater. Chem. A*, 2021, **9**, 11787-11793.
2.   L. Luo, W. Huang, C. Yang, J. Zhang and Q. Zhang, *Front. Phys.*, 2021, **16**, 33500.
3.   J. Mei, Y. Diao, A. L. Appleton, L. Fang and Z. Bao, *J. Am. Chem. Soc.*, 2013, **135**, 6724-6746.
4.   E. Wang, W. Mammo and M. R. Andersson, *Adv. Mater.*, 2014, **26**, 1801-1826.
5.   J.-P. Sun, A. D. Hendsbee, A. a. F. Eftaiha, C. Macaulay, L. R. Rutledge, G. C. Welch and I. G. Hill, *J. Mater. Chem. C*, 2014, **2**, 2612-2621.
6.   L. Dou, Y. Liu, Z. Hong, G. Li and Y. Yang, *Chem. Rev.*, 2015, **115**, 12633-12665.
7.   X. Yong, G. Wu, W. Shi, Z. M. Wong, T. Deng, Q. Zhu, X. Yang, J.-S. Wang, J. Xu and S.-W. Yang, *J. Mater. Chem. A*, 2020, **8**, 21852-21861.
8.   R. Zhao, Y. Min, C. Dou, B. Lin, W. Ma, J. Liu and L. Wang, *ACS Applied Polymer Materials*, 2020, **2**, 19-25.
9.   Y. Pan and G. Yu, *Chem. Mater.*, 2021, **33**, 2229-2257.
10.   X. Liu, L. Nian, K. Gao, L. Zhang, L. Qing, Z. Wang, L. Ying, Z. Xie, Y. Ma, Y. Cao, F. Liu and J. Chen, *J. Mater. Chem. A*, 2017, **5**, 17619-17631.
11.   L. Xiao, B. He, Q. Hu, L. Maserati, Y. Zhao, B. Yang, M. A. Kolaczkowski, C. L. Anderson, N. J. Borys, L. M. Klivansky, T. L. Chen, A. M. Schwartzberg, T. P. Russell, Y. Cao, X. Peng and Y. Liu, *Joule*, 2018, **2**, 2154-2166.
12.   L. Nian, Y. Kan, H. Wang, K. Gao, B. Xu, Q. Rong, R. Wang, J. Wang, F. Liu, J. Chen, G. Zhou, T. P. Russell and A. K. Y. Jen, *Energy Environ. Sci.*, 2018, **11**, 3392-3399.
13.   L. Liu, Y. Kan, K. Gao, J. Wang, M. Zhao, H. Chen, C. Zhao, T. Jiu, A.-K. Y. Jen and Y. Li, *Adv. Mater.*, 2020, **32**, 201907604.
14.   Y. Sun, T. Liu, Y. Kan, K. Gao, B. Tang and Y. Li, *Small Sci.*, 2021, **1**, 2100001.

15. M. Kim, S. U. Ryu, S. A. Park, K. Choi, T. Kim, D. Chung and T. Park, *Adv. Funct. Mater.*, 2020, **30**, 201904545.
16. W. Shi, Y. Guo and Y. Liu, *Adv. Mater.*, 2020, **32**, 201901493.
17. H. Yan, Z. Chen, Y. Zheng, C. Newman, J. R. Quinn, F. Dötz, M. Kastler and A. Facchetti, *Nature*, 2009, **457**, 679-686.
18. T. Lei, X. Xia, J.-Y. Wang, C.-J. Liu and J. Pei, *J. Am. Chem. Soc.*, 2014, **136**, 2135-2141.
19. C. Zhang, Y. Zang, E. Gann, C. R. McNeill, X. Zhu, C.-a. Di and D. Zhu, *J. Am. Chem. Soc.*, 2014, **136**, 16176-16184.
20. Z. Chen, P. Cai, J. Chen, X. Liu, L. Zhang, L. Lan, J. Peng, Y. Ma and Y. Cao, *Adv. Mater.*, 2014, **26**, 2586-2591.
21. W. Wu, Y. Liu and D. Zhu, *Chem. Soc. Rev.*, 2010, **39**, 1489-1502.
22. X. Guo, M. Baumgarten and K. Muellen, *Prog. Polym. Sci.*, 2013, **38**, 1832-1908.
23. J. Mei and Z. Bao, *Chem. Mater.*, 2014, **26**, 604-615.
24. P. Li, L. Xu, H. Shen, X. Duan, J. Zhang, Z. Wei, Z. Yi, C.-a. Di and S. Wang, *ACS Appl. Mater. Interfaces*, 2016, **8**, 8620-8626.
25. L. Ying, F. Huang and G. C. Bazan, *Nat. Commun.*, 2017, **8**, 14047.
26. Y. Gao, Y. Deng, H. Tian, J. Zhang, D. Yan, Y. Geng and F. Wang, *Adv. Mater.*, 2017, **29**, 1606217.
27. Y. Yang, Z. Liu, G. Zhang, X. Zhang and D. Zhang, *Adv. Mater.*, 2019, **31**, 1903104.
28. S. Fratini, M. Nikolka, A. Salleo, G. Schweicher and H. Sirringhaus, *Nat. Mater.*, 2020, **19**, 491-502.
29. J. D. Yuen, J. Fan, J. Seifter, B. Lim, R. Hufschmid, A. J. Heeger and F. Wudl, *J. Am. Chem. Soc.*, 2011, **133**, 20799-20807.
30. J. Lee, A. R. Han, H. Yu, T. J. Shin, C. Yang and J. H. Oh, *J. Am. Chem. Soc.*, 2013, **135**, 9540-9547.
31. B. He, A. B. Pun, D. Zherebetskyy, Y. Liu, F. Liu, L. M. Klivansky, A. M. McGough, B. A. Zhang, K. Lo, T. P. Russell, L. Wang and Y. Liu, *J. Am. Chem. Soc.*, 2014, **136**, 15093-15101.
32. D. Chen, C. Zhong, Y. Zhao, Y. Liu and J. Qin, *Mater. Chem. Front.*, 2017, **1**, 2085-2093.
33. J. Yang, H. Wang, J. Chen, J. Huang, Y. Jiang, J. Zhang, L. Shi, Y. Sun, Z. Wei, G. Yu, Y. Guo, S. Wang and Y. Liu, *Adv. Mater.*, 2017, **29**, 1606162.
34. Y. Wang, H. Guo, A. Harbuzaru, M. A. Uddin, I. Arrechea-Marcos, S. Ling, J. Yu, Y. Tang, H. Sun, J. T. López Navarrete, R. P. Ortiz, H. Y. Woo and X. Guo, *J. Am. Chem. Soc.*, 2018, **140**, 6095-6108.
35. Z. Ni, H. Wang, Q. Zhao, J. Zhang, Z. Wei, H. Dong and W. Hu, *Adv. Mater.*, 2019, **31**, 201806010.
36. Y. Sun, Y. Guo and Y. Liu, *Mater. Sci. Eng. R Rep.*, 2019, **136**, 13-26.
37. J. Huang, S. Lu, P.-A. Chen, K. Wang, Y. Hu, Y. Liang, M. Wang and E. Reichmanis, *Macromolecules*, 2019, **52**, 4749-4756.
38. X. Zhao, H. Cai, Y. Deng, Y. Jiang, Z. Wang, Y. Shi, Y. Han and Y. Geng, *Macromolecules*, 2021, **54**, 3498-3506.
39. T. Mikie and I. Osaka, *J. Mater. Chem. C*, 2020, **8**, 14262-14288.
40. B. Yuan, C. Li, Y. Zhao, O. Gröning, X. Zhou, P. Zhang, D. Guan, Y. Li, H. Zheng, C. Liu, Y. Mai, P. Liu, W. Ji, J. Jia and S. Wang, *J. Am. Chem. Soc.*, 2020, **142**, 10034-10041.
41. Y. Deng, B. Sun, Y. He, J. Quinn, C. Guo and Y. Li, *Angew. Chem.*, 2016, **55**, 3459-3462.

42. Z. Zeng, S. Lee, M. Son, K. Fukuda, P. M. Burrezo, X. Zhu, Q. Qi, R.-W. Li, J. T. L. Navarrete, J. Ding, J. Casado, M. Nakano, D. Kim and J. Wu, *J. Am. Chem. Soc.*, 2015, **137**, 8572-8583.
43. K. Yang, X. Zhang, A. Harbuzaru, L. Wang, Y. Wang, C. Koh, H. Guo, Y. Shi, J. Chen, H. Sun, K. Feng, M. C. Ruiz Delgado, H. Y. Woo, R. P. Ortiz and X. Guo, *J. Am. Chem. Soc.*, 2020, **142**, 4329-4340.
44. C.-L. Chung, H.-C. Chen, Y.-S. Yang, W.-Y. Tung, J.-W. Chen, W.-C. Chen, C.-G. Wu and K.-T. Wong, *ACS Appl. Mater. Interfaces*, 2018, **10**, 6471-6483.
45. Y. Kim, H. Hwang, N.-K. Kim, K. Hwang, J.-J. Park, G.-I. Shin and D.-Y. Kim, *Adv. Mater.*, 2018, **30**, 1706557.
46. J. Huang and G. Yu, *Mater. Chem. Front.*, 2021, **5**, 76-96.
47. I. Osaka, T. Abe, H. Mori, M. Saito, N. Takemura, T. Koganezawa and K. Takimiya, *J. Mater. Chem. C*, 2014, **2**, 2307-2312.
48. W. Hong, B. Sun, C. Guo, J. Yuen, Y. Li, S. Lu, C. Huang and A. Facchetti, *Chem. Commun.*, 2013, **49**, 484-486.
49. H. Hwang, Y. Kim, M. Kang, M.-H. Lee, Y.-J. Heo and D.-Y. Kim, *Polym. Chem.*, 2017, **8**, 361-365.
50. W. Cui, J. Yuen and F. Wudl, *Macromolecules*, 2011, **44**, 7869-7873.
51. W. Cui and F. Wudl, *Macromolecules*, 2013, **46**, 7232-7238.
52. J. W. Rumer, S. Rossbauer, M. Planells, S. E. Watkins, T. D. Anthopoulos and I. McCulloch, *J. Mater. Chem. C*, 2014, **2**, 8822-8828.
53. K. Kawabata, M. Saito, I. Osaka and K. Takimiya, *J. Am. Chem. Soc.*, 2016, **138**, 7725-7732.
54. X. Liu, B. He, C. L. Anderson, J. Kang, T. Chen, J. Chen, S. Feng, L. Zhang, M. A. Kolaczkowski, S. J. Teat, M. A. Brady, C. Zhu, L.-W. Wang, J. Chen and Y. Liu, *J. Am. Chem. Soc.*, 2017, **139**, 8355-8363.
55. C. L. Anderson, N. Dai, S. J. Teat, B. He, S. Wang and Y. Liu, *Angew. Chem. Int. Ed.*, 2019, **58**, 17978-17985.
56. C. L. Anderson, J. Liang, S. J. Teat, A. Garzon-Ruiz, D. P. Nenon, A. Navarro and Y. Liu, *Chem. Commun.*, 2020, **56**, 4472-4475.
57. L. Wang, X. Liu, X. Shi, C. L. Anderson, L. M. Klivansky, Y. Liu, Y. Wu, J. Chen, J. Yao and H. Fu, *J. Am. Chem. Soc.*, 2020, **142**, 17892-17896.
58. C. Zhang and X. Zhu, *Acc. Chem. Res.*, 2017, **50**, 1342-1350.
59. H. Zhang, J.-M. Neudörfl and B. Tieke, *Polym. Chem.*, 2014, **5**, 3754-3757.
60. X. Ji and L. Fang, *Polym. Chem.*, 2021, **12**, 1347-1361.
61. X. Liu, B. He, A. Garzon-Ruiz, A. Navarro, T. L. Chen, M. A. Kolaczkowski, S. Feng, L. Zhang, C. A. Anderson, J. Chen and Y. Liu, *Adv. Funct. Mater.*, 2018, **28**, 201801874.
62. P. Sonar, E. L. Williams, S. P. Singh and A. Dodabalapur, *J. Mater. Chem.*, 2011, **21**, 10532-10541.
63. J. S. Ha, K. H. Kim and D. H. Choi, *J. Am. Chem. Soc.*, 2011, **133**, 10364-10367.
64. Z. Yi, Y. Jiang, L. Xu, C. Zhong, J. Yang, Q. Wang, J. Xiao, X. Liao, S. Wang, Y. Guo, W. Hu and Y. Liu, *Adv. Mater.*, 2018, **30**, 201801951.
65. D.-M. Smilgies, *J. Appl. Crystallogr.*, 2009, **42**, 1030-1034.
66. J. Rivnay, R. Noriega, J. E. Northrup, R. J. Kline, M. F. Toney and A. Salleo, *Phys. Rev. B*, 2011, **83**, 121306.
67. C. Cheng, H. Geng, Y. Yi and Z. Shuai, *J. Mater. Chem. C*, 2017, **5**, 3247-3253.
68. J. Yang, Z. Zhao, H. Geng, C. Cheng, J. Chen, Y. Sun, L. Shi, Y. Yi, Z. Shuai, Y. Guo, S. Wang and Y. Liu, *Adv. Mater.*, 2017, **29**, 201702115.